# Turbofan Engine Blade Pressure and Acoustic Radiation at Simulated Forward Speed

J.S. Preisser,* J.A. Schoenster,* and R.A. Golub†
*NASA Langley Research Center, Hampton, Virginia*
and
C. Horne‡
*NASA Ames Research Center, Moffett Field, California*

**Tests have been conducted on a JT15D-1 turbofan engine both statically and at simulated forward speed in the Ames 12×24 m Wind Tunnel. Both far-field acoustic data and unsteady pressure data from transducers mounted on the fan blades were acquired. Results showed a sound power reduction of about 10 dB in the far-field acoustic levels with simulated forward speed over that measured without forward speed. Blade-mounted transducer results showed rotor-turbulence interaction dominated the noise field at very low speeds while an interaction between the rotor and internal struts dominated at higher speeds. Results are presented to show the effects of varying engine revolutions per minute, changing the angle of attack of the engine inlet to tunnel flow, and mounting an aircraft wing to simulate an installation condition on a actual aircraft.**

## I. Introduction

A NASA intercenter research program is underway with the objective of developing the understanding and techniques necessary for proper ground simulation of fan noise in flight. The core of the program involves testing a heavily instrumented JT15D-1 turbofan engine on a static test stand, in a wind tunnel, and in flight. Initial results have recently been reported[1] on the comparison of several inflow control devices used in static testing which were designed to simulate the inflow and noise environment that would be encountered in flight. An initial series of flight tests have been conducted with a JT15D-1 mounted under the wing of a modified OV-1B Mohawk aircraft and the data are currently being analyzed. These data, along with future flight data, will serve as the criteria for evaluating the various ground-based flight-simulation techniques. This paper will present some results from recent tests of the engine tested both statically and at simulated forward speed in a wind tunnel.

Tests of the JT15D-1 were performed at the Ames Research Center in two facilities: the Outdoor Test Stand and the 12×24 m Wind Tunnel. Similar engines have previously been tested in these facilities[2-4] and various amounts of acoustic and engine performance data were obtained. Generally, the results showed a reduction in the noise level at blade passage frequency (BPF) with simulated forward speed. This is consistent with the generally accepted belief[5] that forward speed reduces streamtube contraction and consequently lessens the intensity of ingested turbulence and other unsteady disturbances, which in turn, decreases rotor-turbulence interaction noise. The size of the reduction of the BPF with forward speed, however, has not been as great as theory[6] would predict for the JT15D, and a residual tone noise remained.

The present tests were undertaken with a much more heavily instrumented engine in order to study in greater detail the effects of forward speed on fan noise. In particular, several dynamic pressure transducers were mounted on the fan blades. This paper will present results obtained from one of the transducers: a transducer near the leading edge of the blade was selected since it displayed general characteristics representative of this engine. Further results, including those from other transducer locations, may be found in Ref. 7. The blade-mounted transducers (BMTs) are a relatively new tool for acoustic investigations, and have been used in evaluating inflow control devices and in postulating the importance of various noise source mechanisms.[1] This is the first known application of BMTs on a turbofan engine in a wind tunnel.

The purpose of this paper is to study the effects of forward speed on acoustic radiation at the blade passage frequency, to identify the potential noise mechanisms which may dominate in flight, to assess the effect of angle of attack on BPF directivity, and to ascertain any installation effects which may be present for the flight tests of the OV-1B/JT15D-1 aircraft/engine configuration.

## II. Test Description

### Test Engine

The test engine was a JT15D-1 turbofan engine manufactured by Pratt & Whitney Aircraft of Canada Limited. The engine is a twin spool, front fan jet propulsion engine which has a full length annular bypass duct. It has a nominal bypass ratio of 3.3 and a maximum thrust capability of 9790 N (see Table 1 for design features).

The fan is 53.3 cm in diameter and has 28 blades (see Figs. 1 and 2). The fan is followed by a stator assembly consisting of a bypass stator which has 66 vanes and a core stator which has 71 vanes. The latter is the only predominant difference between a production JT15D-1 engine (which has 33 core-stator vanes) and the instrumented engine used in these tests. The modified core stator has more blades and has been set back aft of the rotor blade root a distance of 0.63 fan blade root chords (as compared to 0.28 chords for a production engine) so that both the fan rotor/core-stator interaction tone would be acoustically cut off and the broadband noise diminished. The next rotating blade assembly is the compressor, which is a combination axial-centrifugal compressor having 16 blades in the leading axial part of the unit.

As shown in Fig. 3, the engine core is supported by six structural struts which are located in the intermediate case of the engine. These supports traverse both the compressor and bypass ducts to tie the core to the outer wall of the engine intermediate case. As shown in Fig. 2, these struts are located directly behind the stator assembly.

The test engine was fitted with a muffler to reduce the aft radiated bypass duct noise. This was considered necessary to minimize any possible contamination with the front-end

Presented as Paper 81-0096 at the AIAA 19th Aerospace Sciences Meeting, St. Louis, Mo., Jan. 12-15, 1981; submitted Feb. 24, 1981; revision received April 26, 1982. This paper is declared a work of the U.S. Government and therefore is in the public domain.

*Aerospace Engineer, Noise Control Branch, ANRD. Member AIAA.
†Aerospace Engineer, Noise Control Branch, ANRD.
‡Aerospace Engineer, Low Speed Aircraft Research Branch, AD.

**Table 1 JT15D-1 design features**

| | |
|---|---|
| Maximum fan speed, rpm | 16,000 |
| Fan pressure ratio | 1.5 |
| Bypass ratio (max) | 3.3 |
| Rotor blades | 28 |
| Rotor diameter, m | 0.533 |
| Hub/tip ratio | 0.405 |
| Bypass stator vanes | 66 |
| Core stator vanes | 71[a] |
| Bypass rotor-stator spacing | 1.83 |
| Core rotor-stator spacing | 0.63[b] |
| Maximum compressor speed, rpm | 32,760 |
| Core exhaust area, $m^2$ | 0.051 |
| Bypass exhaust area, $m^2$ | 0.092 |

[a] Production engine has 33 core-stator vanes. [b] Production engine core-stator spacing is 0.28.

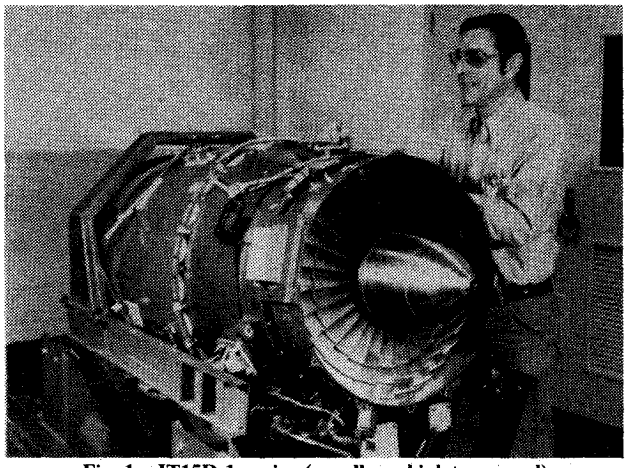

**Fig. 1 JT15D-1 engine (nacelle and inlet removed).**

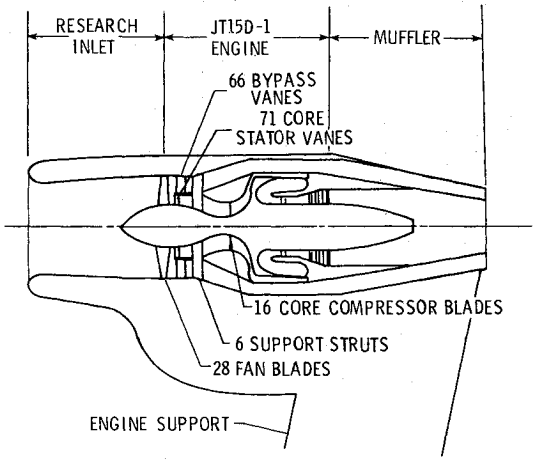


**Fig. 2 Cross-section sketch of JT15D-1 test configuration.**

radiated fan noise measurements of interest in the present investigation. The muffler was designed so that the bypass and core exit areas remained the same as in a production engine.

### Test Facilities and Setup

The instrumented JT15D-1 engine was tested in two different facilities at the Ames Research Center. One was the 12×24 m Wind Tunnel and the other was the N-249 Outdoor Test Stand.

*Wind Tunnel*

Photographs of the engine in the wind tunnel are presented in Fig. 4. For all configurations tested, the JT15D-1 engine was mounted on a support pylon 4.57 m above the tunnel floor. The pylon was connected to a turntable which could yaw the entire assembly to obtain angle-of-attack effects. The test section floor and walls in the immediate area surrounding the engine were lined with a 7.62-cm-thick layer of polyurethane foam. The foam was intended to minimize reverberant reflections.

The noise measurements were made with ten microphones utilizing two types of microphone systems: a microphone traversing rail (Fig. 4a) and stationary microphone stands (Figs. 4a and 4b). All of the microphones were equipped with nose cones and were pointed into the direction of the tunnel airflow. Nine of the microphones were mounted on fixed

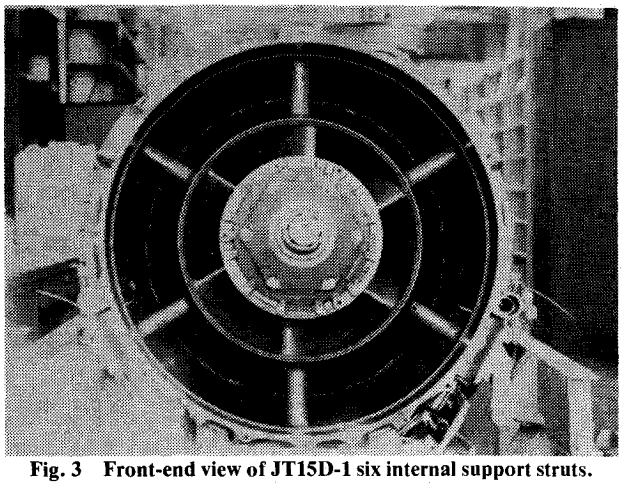

**Fig. 3 Front-end view of JT15D-1 six internal support struts.**

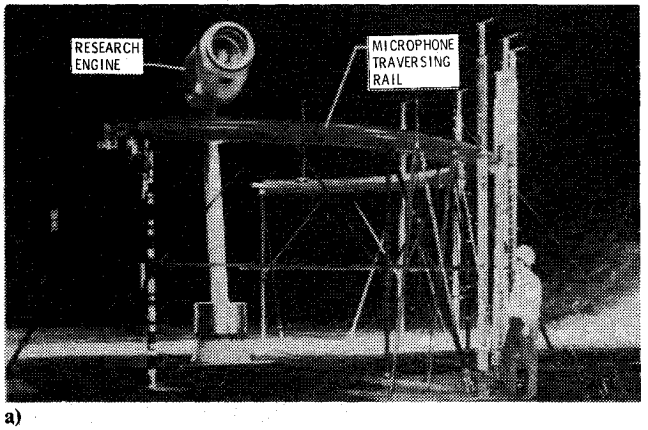


a)

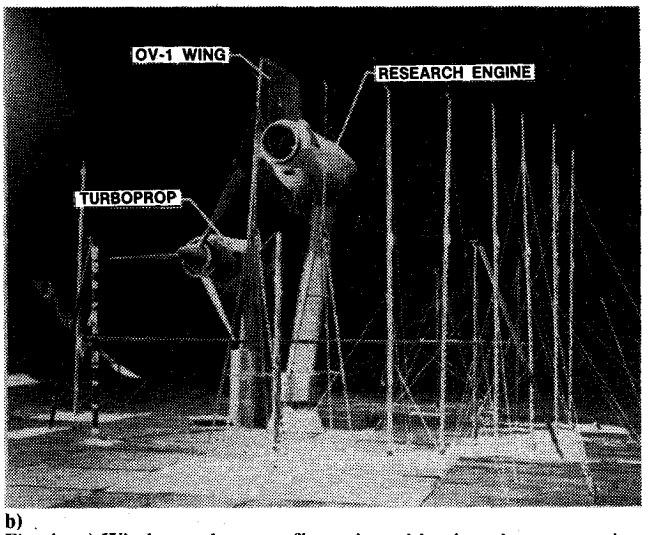


b)

**Fig. 4 a) Wind tunnel test configuration with microphone traversing rail. b) Wind tunnel test configuration with OV-1B turboprop/wing assembly.**

poles which were adjusted to the same height as the engine centerline (4.57 m) and positioned around the engine on a 4.05-m-radius arc measured from the centerline point of the engine fan face. The tenth microphone when used was mounted on a weather-vaning support attached to a 3.66-m-radius traversing rail (see Fig. 4a). This microphone was also positioned at the height of the engine centerline, and traversed an arc from 0 to 137 deg from the inlet axis.

During some of the tests, a wing and turboprop engine from an OV-1 Mohawk aircraft were mounted in the wind tunnel (see Fig. 4b). The turboprop was securely fastened in a fixed position so that it would not rotate in the tunnel flow. Unpublished hot film data taken under the wing of the OV-1 in flight had indicated a rotating turboprop would cause an inflow distortion problem for the JT15D. The purpose of the present test was to investigate the potential flowfield effects of the wing and stationary turboprop upon the JT15D-1 engine inlet and the inlet radiated noise field. This test configuration was a simulation of the OV-1B/JT15D-1 research aircraft configuration which will be used to provide flight data.

For the present investigation, tests were run at five tunnel speeds from tunnel-off conditions to 56 m/s, and at angles of attack of 0 and 8 deg.

*Outdoor Test Stand*

The test runs at the N-249 Outdoor Test Stand (shown in Fig. 5) were patterned after the wind tunnel runs. The same engine/nacelle/pylon structures were utilized, resulting in the same engine centerline height of 4.57 m. The same pole-mounted and traversing microphones were used and positioned identically as they were in the wind tunnel. No OV-1 wing/engine simulation tests were performed at the outdoor test stand. The test runs were performed early in the morning when the winds were less than 3 m/s.

**Instrumentation and Data Processing**

*Blade-Mounted Systems*

Miniature Kulite pressure transducers were mounted at several locations on two of the 28 fan blades of the JT15D engine to measure the fluctuating pressure on the surface of the blades. Data from these transducers were transmitted from the hub of the fan to an antenna in the inlet duct wall, demodulated, and recorded on magnetic tape as analog pressure signals (see Fig. 6). The capability of the transducers to measure fluctuating pressures in the environment of the rotating blades has been evaluated and is reported in Ref. 8.

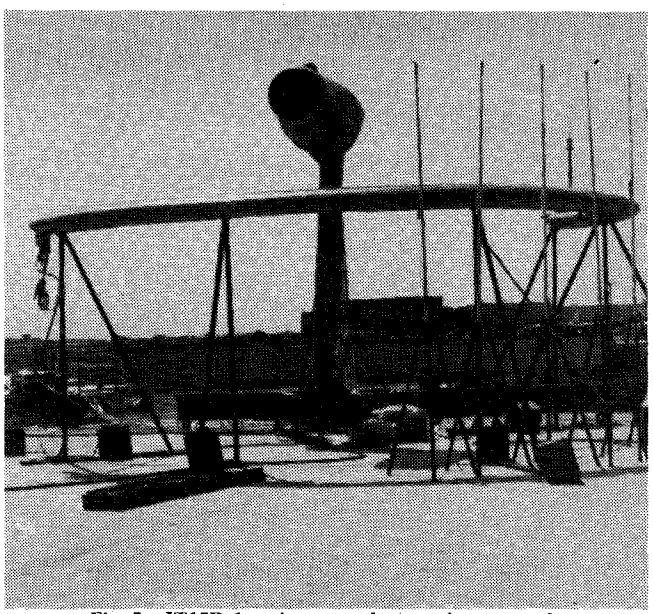

**Fig. 5 JT15D-1 engine at outdoor static test stand.**

Data from an identical system were obtained at the NASA Lewis Research Center and some of these data have been reported in Ref. 1. The basic system is designed to measure pressures from 20 Hz to 20 kHz with a sensitivity of $1.451 \times 10^{-4}$ V/Pa (1 V/psi). A typical transducer installation on a fan blade is shown in Fig. 7. The transducer sensing diameter was 1 mm.

Data from a single transducer (designated as Transducer H in Ref. 7) are presented in this paper. This transducer is located on the "pressure side" of the blade approximately 1.9 cm from the duct wall and 4 mm from the leading edge of the blade.

The data were analyzed using both a constant bandwidth spectral analyzer and a specially developed computer program. The computer program followed a procedure outlined by Hanson.[5] The results are presented as follows: 1) A signal (optical) is used to generate an electrical pulse for each revolution of the instrumented fan blade. Using this signal as a reference, the data are digitized at a rate of 360 points per revolution. These data are then analyzed by an FFT computer program to determine the spectral levels of the signal. 2) Using the 1-per-revolution signal to locate top-dead-center of rotation for the instrumented blade, the data are then ordered by angle (each point representing 1 deg) around the duct circumference. The mean value and the standard deviation of the pressure are calculated and plotted as a function of the angle around the circumference (the angles are positive counterclockwise looking into the inlet). 3) The mean value signal is then analyzed for the harmonic frequency content of the pressure. The program automatically calculates 90 orders of the rotational frequency in one-fourth rotational frequency bandwidths irrespective of the frequency of rotation.

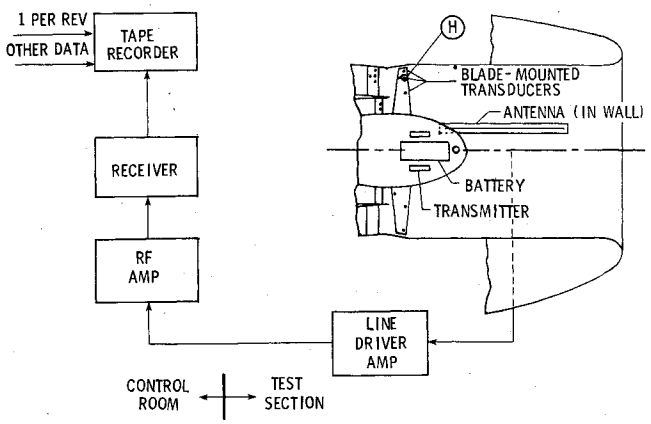


**Fig. 6 Sketch of JT15D-1 showing pressure transducer locations and telemetry and recording systems.**

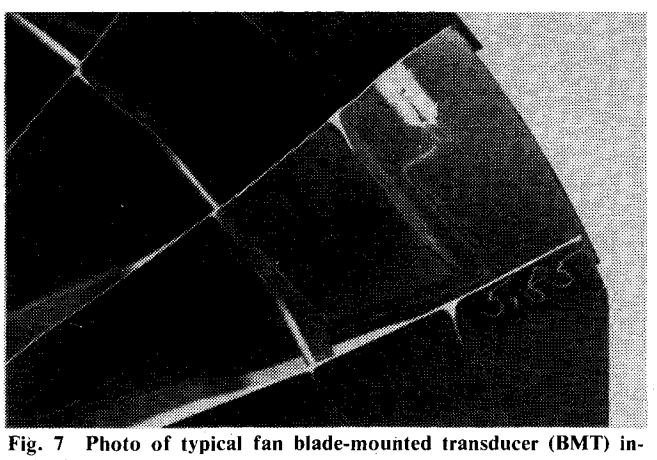

**Fig. 7 Photo of typical fan blade-mounted transducer (BMT) installation.**

*Far-Field Acoustic Systems*

The noise measurements were made by ten 1.27-cm-diam microphones equipped with nose cones. All acoustic data were unfiltered and recorded at 30 in./s on magnetic tape for post-test data analysis. For this report, acoustic results using the traversing microphone are presented to show the effects of forward speed. These data are presented in the form of BPF directivity and were analyzed at a constant bandwidth of 50 Hz. Effects of engine speed, angle of attack, and OV-1 installation effects are discussed with the aid of data obtained by the stationary microphones. These data are presented in the form of narrow-band spectra (either 25 or 50 Hz bandwidth) and directivity patterns of BPF tones.

No acoustic response corrections or adjustments due to the various nose cone angle of incidences were made for this report, although a study has been completed[9] to show this effect relative to static and flight measurement systems used in other portions of the program. The corrections are functions of frequency and incidence angle and are of such a magnitude as not to affect the conclusions drawn in this report. No corrections were made to the data for room effects or for tunnel flow convection on the acoustic radiation patterns.

## III. Results and Discussion

Results are presented on the effects of engine rpm, forward speed, and angle of attack. In addition, the question of installation effects applicable to a subsequent flight test program employing the JT15D-1, is addressed. Acoustic results are presented in the form of narrow-band spectra, sound power, and directivity patterns of the blade passage frequency (BPF). Fan blade transducer results are presented as fluctuating pressure spectra, signal enhanced pressure spectra, and circumferential distributions of the mean pressure signal and its standard deviation.

### Effects of Engine rpm

A typical set of data showing operating fan speed range with associated core compressor speeds obtained during an engine power sweep are shown in Fig. 8. Additional scales are also presented for fan blade passage frequency and core blade passage frequency, based on 28 fan blades and 16 axial core compressor blades, respectively (refer to Fig. 2). Because of the twin-spool design feature of the JT15D there is no linear relationship between the two speeds. During the present tests, data were obtained over an engine operating range from just above idle to takeoff power. This resulted in a wide range of flow-relative Mach numbers at the fan blade tip from subsonic to supersonic. Most of the results presented in this paper are for a typical approach power setting of 10,500 rpm, which resulted in a high subsonic tip Mach number.

*Acoustic Spectra*

Figure 9 presents narrow-band sound pressure spectra (50 Hz bandwidth) for various fan speeds. The spectra were obtained in the tunnel from a fixed microphone located 48 deg from the engine inlet axis. For these data, the wing was present. Although the wind tunnel was not operating at this time, natural convection and recirculation of the engine exhaust caused a slight tunnel flow which varied from 2 m/s at the low fan speeds to 7 m/s at the high. These data are characterized by a broadband base which increases in level

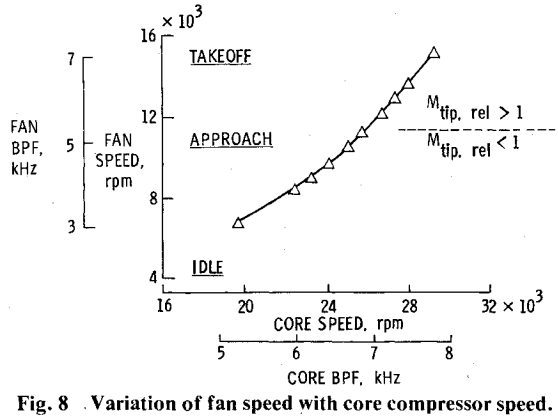


**Fig. 8 Variation of fan speed with core compressor speed.**

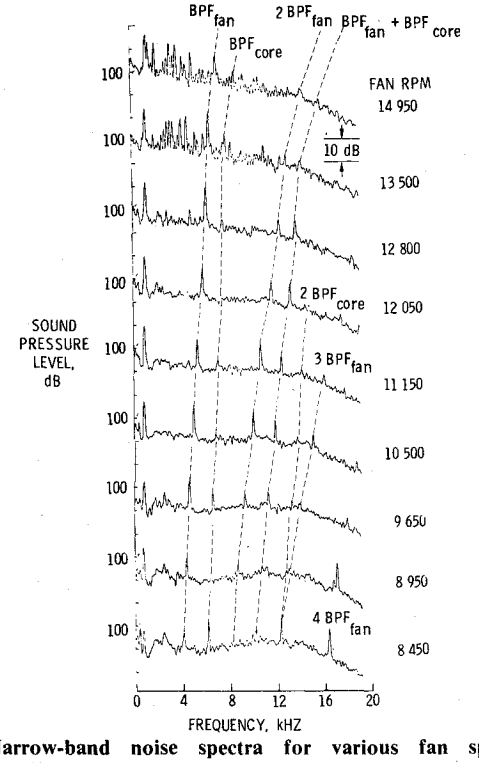


**Fig. 9 Narrow-band noise spectra for various fan speeds; microphone 48 deg from inlet axis, minimum tunnel speed, engine/wing configuration, 50 Hz bandwidth.**

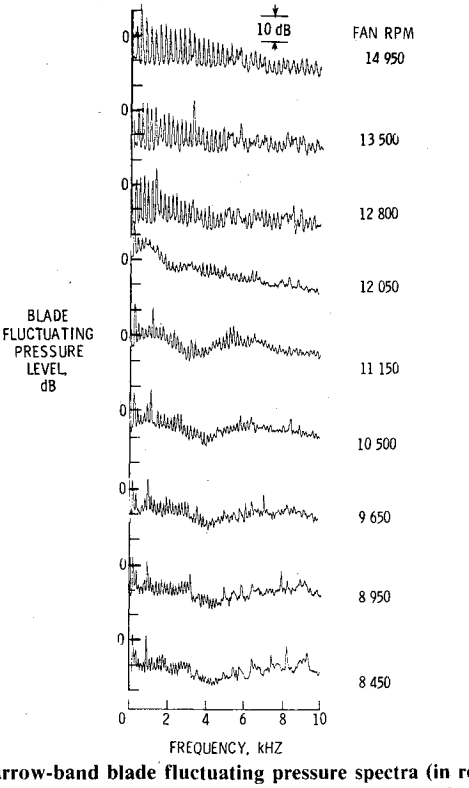


**Fig. 10 Narrow-band blade fluctuating pressure spectra (in relative dB) for various fan speeds, BMT H, minimum tunnel speed, engine/wing configuration, 25 Hz bandwidth.**

with increasing fan speed and by sharp peaks superimposed on the base. With the aid of the previous figure, these peaks were identified as the fan blade passage frequency, the core compressor blade passage frequency, and various harmonics and combination tones of both. The peak which is evident in all spectra at 1000 Hz or less is believed to be lip noise associated with the particular engine muffler design used in this study. The data show a strong fan BPF tone at all fan speeds for this particular configuration; a 2-BPF tone and a combination tone whose frequency is the sum of the core and fan BPFs are strong only in the midspeed range. Note that the level of the core compressor tone is greatly enhanced for the 8450-rpm case. At this fan speed, there is a merger of the 2-BPF core tone with the 3-BPF fan tone and a subsequent amplification in level of the core BPF.

In general, the acoustic data of Fig. 9 can be grouped into two categories: the two top spectra where many special peaks are evident and the remaining seven spectra. Since Fig. 8 shows the fan blade tip speed to be supersonic at these higher fan speeds, multiple pure tones (MPTs) at other frequencies are generated as well as a strong BPF tone. The remaining spectra have no MPTs but display a strong BPF tone. Recall the core stator was modified so that the rotor/core-stator interaction would be cut off for the entire operating range of the engine. Hence other noise source mechanisms must contribute to the BPF at the lower fan speeds.

*BMT Spectra*

Figure 10 presents narrow-band fan blade pressure spectra (25 Hz bandwidth) for the identical engine operating conditions of the previous figure. These data were taken by BMT H, a transducer on the pressure side of the blade near the tip but not in the inlet boundary layer. Note that a frequency scale is shown on the abscissa, although it should be remembered that the transducer is on a rotating blade and therefore does not measure the same spectral energy content as would a stationary transducer, such as far-field microphone. It should be mentioned that the BMT data represent a single point measurement on a given blade and may not be representative of the chordwise and spanwise blade loading. Hence it is not possible to quantitatively relate a single BMT measurement to the far-field acoustics. In this paper, BMT spectral data will be presented on a relative dB basis and changes in BMT response with changing test conditions will be viewed in a qualitative sense only. A further explanation of BMT spectra will be given in a subsequent section of this paper.

In general, the data of Fig. 10 can be placed in three different groupings. The top three spectra are all characterized by large multiple harmonics, probably owing to the supersonic tip speed and the rotating uneven shock structure caused by the fan with its randomly different blade-to-blade spacing. The fourth spectrum is different from the rest in that the broadband noise rises significantly (especially at the low frequencies) to the extent that the harmonics are almost obscured. This spectrum corresponds to a transonic tip speed. The lower five spectra are similar in that there is a broadband base with many harmonics a few dB higher, two of which (in the frequency range 0-2 kHz) are significantly higher than the rest. The meaning and significance of these two will be discussed later. It should be kept in mind that energy over a wide range of frequencies on the BMTs can contribute to the energy of the BPF and its harmonics in the far field.

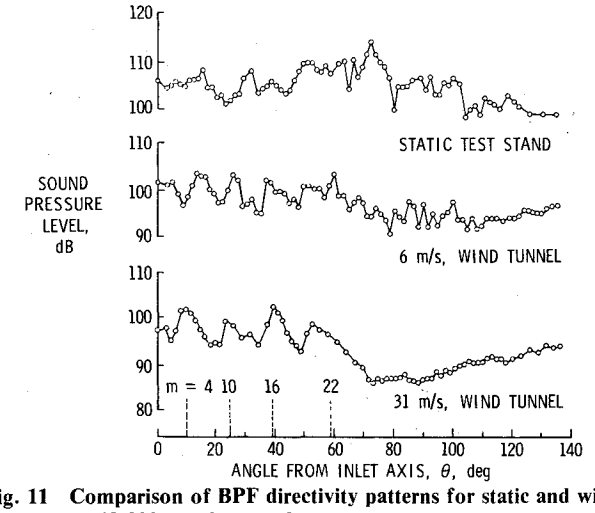


**Fig. 11 Comparison of BPF directivity patterns for static and wind tunnel tests; 12,000 rpm fan speed.**

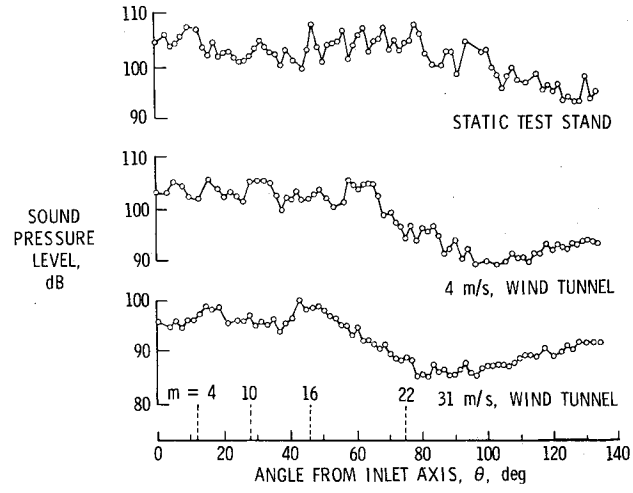


**Fig. 12 Comparison of BPF directivity patterns for static and wind tunnel tests; 10,500 rpm fan speed.**

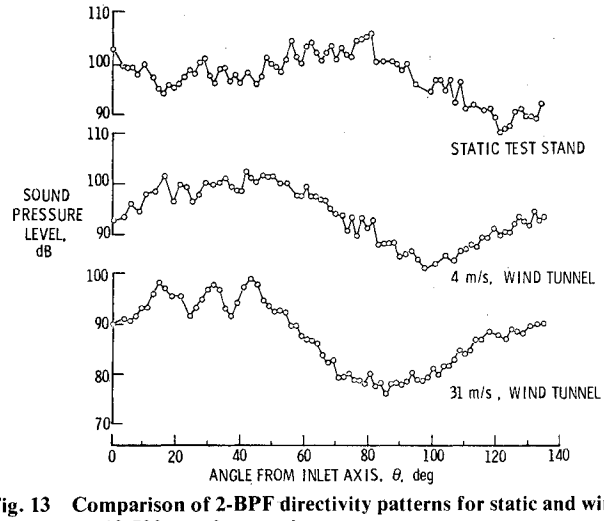


**Fig. 13 Comparison of 2-BPF directivity patterns for static and wind tunnel tests; 10,500 rpm fan speed.**

**Effects of Forward Speed**

*Far-Field Directivity*

Directivity patterns of the blade passage frequency at fan speeds of 12,000 and 10,500 rpm are presented in Figs. 11 and 12, respectively. The directivity of twice the blade passage frequency for the 10,500-rpm case is presented in Fig. 13. For all these figures, the wing was not installed, the angle of attack was 0 deg, and the bandwidth of analysis was 50 Hz. Data are presented for the static test case and for the wind tunnel on and off cases. The data were obtained by the traversing mechanism described in a previous section of this paper. Each data point represents a 2-s average of the tone level as the microphone was moving. This time corresponded to about a 2-deg angular sweep.

In general, the data show the highest levels for the static test case. Also, the greatest data scatter occurs for the static test. This is consistent with studies of other investigators, wherein the interaction of the fan rotor with ingested atmospheric turbulence, ground vortices, and test stand wakes result in high levels of so-called rotor-turbulence interaction noise. The high levels result from a sizable streamtube contraction of the ingested turbulence which becomes chopped by the high-speed fan blades. The random nature of this interaction produces an unsteadiness in fan speed and spatial and temporal variations in the generation and subsequent radiation of the acoustic field.

In the wind tunnel, even with the tunnel off, the recirculation of air and exhaust gases produce a measurable airflow (from 4 to 6 m/s for the data shown), which has a significant effect on the measured directivity. The airflow has a straightening effect on the streamlines and less contraction and turbulence intensification occurs. This effect is in addition to lower turbulence levels in the tunnel compared to outside.[6] The net result is a decrease in the noise field, the largest reductions being in the range between 60 and 100 deg. With a further increase in simulated forward speed or tunnel airflow, additional reductions in the noise field occur. At a tunnel speed of 31 m/s, lower levels and less data scatter are evident. Local peaks emerge in the directivity pattern at angles less than 60 deg from the inlet axis. With rotor-turbulence interaction substantially reduced at this tunnel speed, other noise source mechanisms become dominant. The peaks in the directivity suggest propagating acoustic modes. As described in Ref. 10, an acoustic mode is identified by its circumferential, $m$, and radial, $\mu$, order. The $m$ order of the mode for the BPF tone generated when $V$ stationary vanes or struts interact with $B$ rotating blades is given by

$$m = B - KV$$

where $K$ is any integer.

The criteria for propagation is the cutoff ratio $\xi$ given by

$$\xi = \frac{BM_t}{k'_{m,\mu}(1-M^2)^{1/2}}$$

where $M_t$ and $M$ are the rotor tip and duct flow Mach numbers, respectively, and $k'_{m,\mu}$ is the mode eigenvalue for the cylindrical duct. A given mode will propagate down the duct if $\xi > 1$ and will decay exponentially if $\xi < 1$. Each propagating mode will radiate a strongly directional acoustic field. Reference 11 has shown that for a flanged duct with flow in the far field equal to that in the duct (an approximation to the present situation) the principal lobe peak can be expressed as a function of cutoff ratio, as follows:

$$\theta_p = \cos^{-1}\left\{\frac{(1-M^2)[1-1/\xi^2]}{1-M^2[1-1/\xi^2]}\right\}^{1/2}$$

The principal lobe peak was calculated for values of $K = 1$, 2, 3, and 4 and $V = 6$. (The reason for this choice for $V$ will become apparent when the blade-mounted transducer data is reviewed in later sections.) Good agreement was obtained between the calculated peaks and the experimental data of Fig. 11 at 12,000 rpm for the resulting $m$ values of 22, 16, 10, and 4. For this fan speed, values of rotor tip and duct flow Mach numbers were taken to be 1.00 and 0.25, respectively, based on JT15D data presented in Ref. 12. For a fan speed of 10,500 rpm, the interpretation is not as clear. In fact, the peak for the $m = 22$ mode is not discernible at all. Hence conclusions for propagating modes based on far-field directivity peaks are not solidly supported for all fan speeds. Also, higher-order radial modes and counter-rotating or negative mode numbers were not considered. In addition, refraction and inlet shape effects can alter the directivity. Nevertheless, the lobe peaks which do appear in the forward quadrant are separated in increments of $\theta$ that correspond to separations in values of $m$ equal to 6.

*Sound Power*

Narrow-band sound power reduction at blade passage frequency due to forward speed is presented in Fig. 14. The data are for a fan speed of 10,500 rpm with the engine alone at 0 deg angle of attack. These data are the result of integrating the traversing microphone sound pressure levels over the forward arc from 0 to 90 deg and are presented relative to the static test case result. Sound power shows a sudden decrease with about 10-m/s tunnel flow followed by a slight decrease thereafter. As suggested previously, this sudden decrease is most likely due to a lessening of streamtube contraction and associated transverse turbulence intensification with forward speed. This drop in rotor-turbulence interaction, which is on the order of 10 dB, uncovers other noise sources for speeds larger than 10 m/s. A theoretical model[6] of sound power reduction at the source with forward speed for the JT15D engine in the Ames 12×24 m Wind Tunnel is also shown on Fig. 14. The theory considers only rotor-turbulence interaction in the fan noise modeling, and hence shows more dramatic reductions.

*Blade-Mounted Transducer Spectra*

Narrow-band spectra of the blade-mounted transducer signal is presented in Fig. 15. The data correspond to the same static and wind tunnel tests as were presented in Fig. 12. The spectra levels are presented on a relative dB basis. In addition to the frequency scale, a harmonic order scale is also shown. That is, the transducer on the rotating blade senses variations

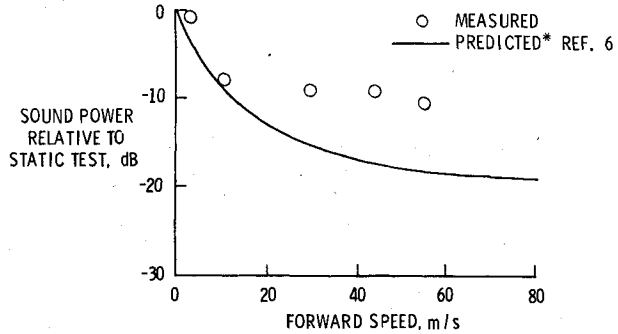


**Fig. 14 Variation of acoustic sound power with forward speed; 10,500 rpm fan speed (*predicted levels are for rotor/turbulence interaction only).**

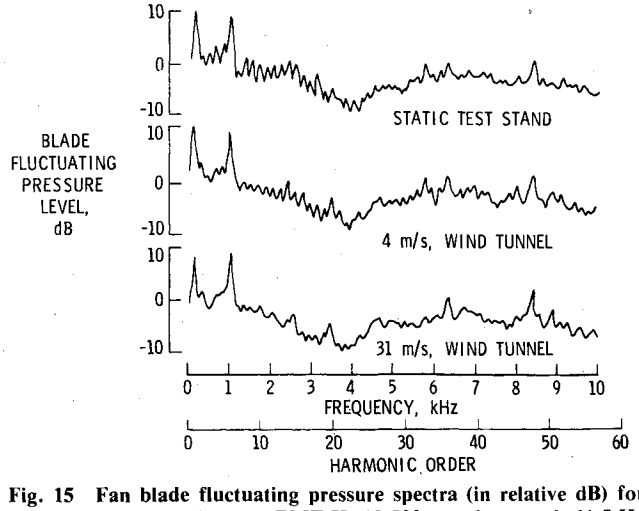


**Fig. 15 Fan blade fluctuating pressure spectra (in relative dB) for static and wind tunnel tests, BMT H, 10,500 rpm fan speed, 61.5 Hz bandwidth.**

in aerodynamic pressure in the circumferential direction as it rotates. Hence the spectrum represents a Fourier decomposition of the steady circumferential variations in the blade pressure response to the flowfield at the fan face. For the spectra shown in this figure the fan speed was 10,500 rpm or 175 rps. A harmonic order of 1 would therefore correspond to 175 Hz. Higher harmonic orders then become multiples of 175 Hz. In addition to steady circumferential distortion, unsteady distortion due to random disturbances, such as ingested atmospheric turbulence, may be present. These unsteady distortions show up as spatial and temporal variations in the transducer signal and may be distributed across many harmonic orders in the spectra.

For all three spectra in Fig. 15, the harmonic orders of 1 and 6 are seen to be dominant. The harmonic order of 1 shows a slight decrease with increasing forward speed; the harmonic order of 6 is relatively invariant with forward speed. In addition to the first and sixth order, the static test case has prominant peaks for all orders up through 20. These higher harmonic orders have levels that also decrease with increasing forward speed. For orders higher than 20, the three spectra are very similar.

The source of the first-order distortion is not clear at the present time. It is not surprising it is present, however, since any slowly varying circumferential variation in the mean pressure field would result in this type of distortion and most likely the engine, nacelle, and installation do not have perfect cylindrical symmetry. The source of the sixth-order distortion, as has been previously suggested in Ref. 1, is believed to be due to the six cylindrical support struts that were shown in Fig. 3. These struts would produce a spatially varying potential field at the fan face; the rotating fan blade would cut through the cyclic field, producing a highly coherent acoustic signal. The appearance of a strong sixth-order harmonic appears for all subsonic fan speeds presented in Fig. 10, as one would expect for a potential field distortion of this type.

It should be noted that fluctuating pressures at all frequencies on the blade-mounted transducers can potentially contribute to the blade passage frequency and its harmonics in the far field, depending on whether the cut-on criteria, $\xi > 1$, is satisfied. For the 10,500 fan speed case, $m = 23$ and below would be cut on; for the 12,000 rpm case, $m = 25$ and below would be cut on. Hence, for both these cases, the strong sixth-order circumferential variation on the blade-mounted transducer would interact with the 28 fan blades to produce acoustically propagating modes, while the first-order circumferential variation combination with the 28 would be cut off.

In view of the blade-mounted transducer spectra and the previously presented acoustic results, it is believed that for the static test stand and for the wind tunnel at simulated forward speeds less than 10 m/s, the acoustic far field is dominated by the random ingestion of turbulence. For tunnel speeds greater than 10 m/s, turbulence cleanup is accomplished, rotor-turbulence sound power production is down 10 dB, and a highly coherent directional field due primarily to the interaction of the rotor with the six internal structural struts most likely becomes the prominant noise source mechanism.

*Signal Enhancement*

The effect of forward speed on the blade pressure spectra as just discussed is further delineated through signal enhancement of the blade pressure signal. Using the optical sensor pulse described in a previous section to determine the angular position of each particular blade and blade transducer in time, the signal was ensemble averaged over 1000 revolutions. The transform of the averaged waveform was then performed. This process removes the pressure variations caused by random distortions and "enhances" those that are regular and periodic in the circumferential direction. The ensemble averaged signal and its standard deviation are shown in Fig. 16 and the signal enhanced pressure spectra are shown in Fig. 17.

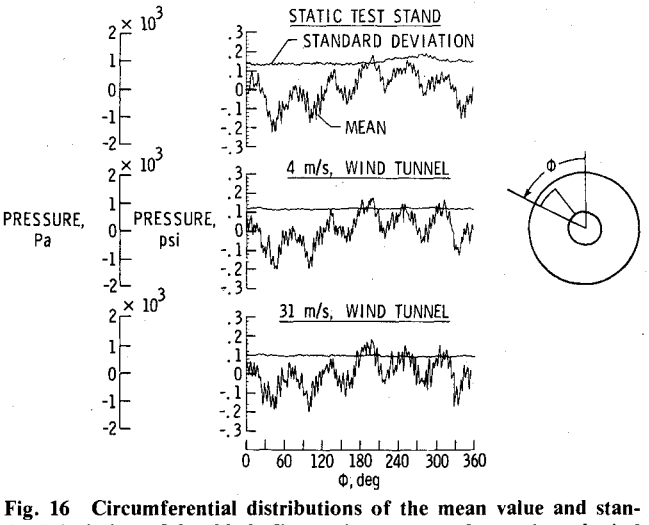


**Fig. 16 Circumferential distributions of the mean value and standard deviation of fan blade fluctuating pressure for static and wind tunnel tests; BMT H, 10,500 rpm fan speed, 1000 revolutions.**

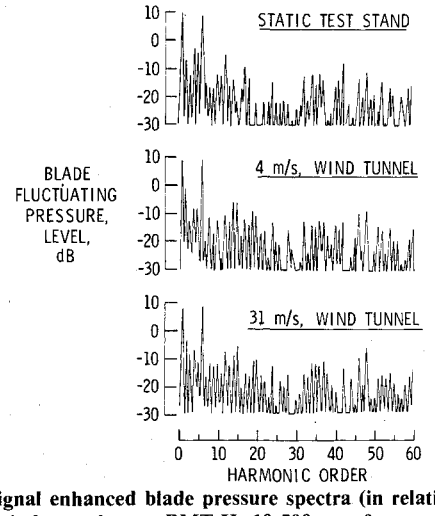


**Fig. 17 Signal enhanced blade pressure spectra (in relative dB) for static and wind tunnel tests; BMT H, 10,500 rpm fan speed, 61.5 Hz bandwidth.**

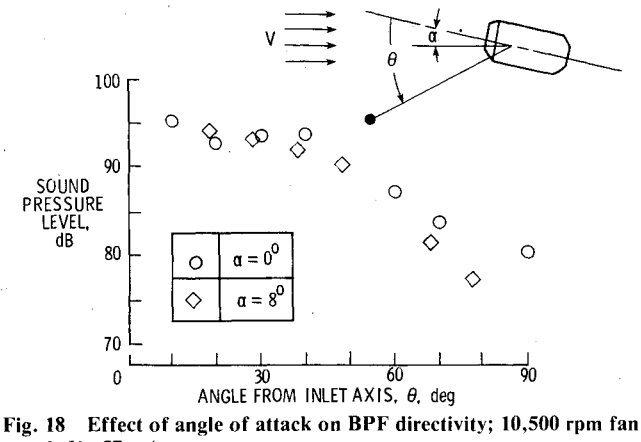


**Fig. 18 Effect of angle of attack on BPF directivity; 10,500 rpm fan speed, $V = 57$ m/s.**

The averaged waveforms clearly show the first- and sixth-order variation evident in the spectra. The first-order variation is seen to result from a higher pressure near the bottom of the duct and a lower pressure near the top. The sixth-order variation is superimposed on this and the position of the six peaks is independent of forward speed, again being consistent with the assumption of being associated with the six structural support struts. In addition, a 66-per-revolution variation is also superimposed. The 66 is undoubtedly due to

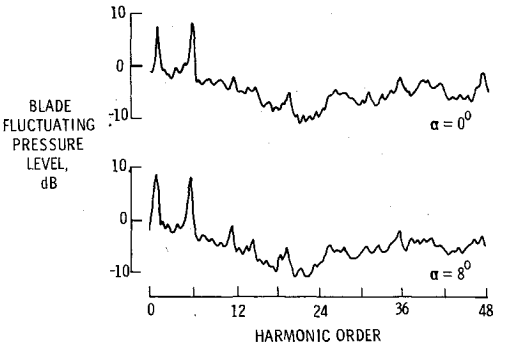


**Fig. 19 Effect of angle of attack on blade fluctuating pressure spectra (in relative dB); BMT H, 10,500 rpm fan speed, $V = 57$ m/s, 61.5 Hz bandwidth.**

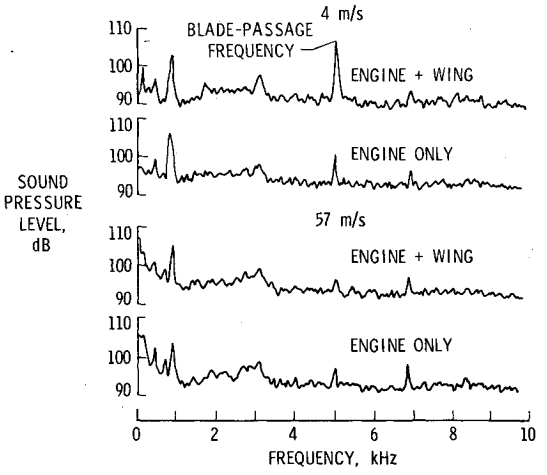


**Fig. 20 Effect of the OV-1 wing on narrow-band sound pressure level; microphone 38 deg from inlet axis, 10,500 rpm fan speed, 25 Hz bandwidth.**

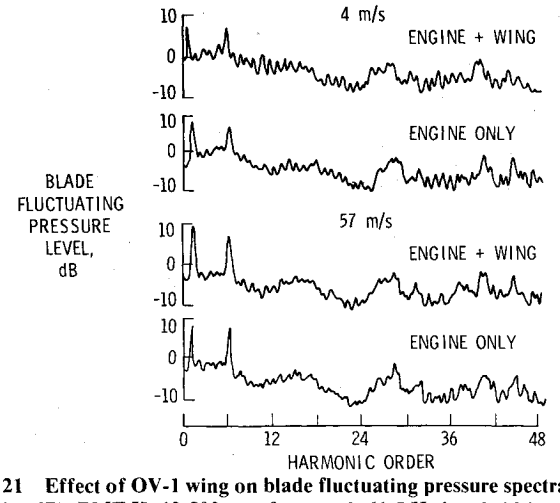


**Fig. 21 Effect of OV-1 wing on blade fluctuating pressure spectra (in relative dB); BMT H, 10,500 rpm fan speed, 61.5 Hz bandwidth.**

the 66 fan bypass vanes which are located a short distance downstream of this particular transducer. The averaged waveforms both in level and shape, are very much like those measured in Ref. 1, using a similar transducer system on a similar engine.

The standard deviation, being a measure of the randomness of the signal, shows a difference with forward speed, as expected. The static test data has the largest standard deviation and is not uniformly distributed. It is uncertain as to why a bump in the data occurs near the 270-deg position; however, any crosswind present during the static test could cause a variation on either side of the duct.

Signal enhanced pressure spectra for the data of Fig. 16 are presented in Fig. 17. The data show significant decreases in level at all harmonic orders, except for those orders of 1 and 6. The levels of the first and sixth order remain virtually identical with the levels of the unenhanced spectra of Fig. 16, indicating the first and sixth order are due to well-defined, steady, periodic distortions.

### Effects of Angle of Attack

*Far-Field Directivity*

The effect of engine angle of attack on blade passage frequency directivity is presented in Fig. 18. Results are shown for angles of attack of 0 and 8 deg. The latter position is a typical value for the flight test portion of the program involving the OV-1B aircraft. For these data, neither the wing nor the traversing microphone and rail were present. The results show very little difference in the far-field BPF directivity with angle of attack. This agreement is consistent with the findings of Ref. 3.

*Blade-Mounted Transducer Spectra*

The effect of engine angle of attack on the fan blade transducer pressure spectra is presented in Fig. 19. These data show virtually no difference at all in either the levels of the peaks or the broadband base upon which the peaks are superimposed. Hence the BMT results support the acoustic results of the previous figure.

### Installation Effects

*Acoustic Spectra*

In Fig. 20 is presented narrow-band spectra at a location 38 deg from the inlet axis showing the effect of wing-in/wing-out and tunnel-on/tunnel-off at a fan speed of 10,500 rpm and an angle of attack of 8 deg. The wing used in this study was from an OV-1 aircraft, similar (but having a slightly shorter wing span) to the aircraft that is being used in the flight portion of the program. The tunnel-off case has a slight forward speed of about 4 m/s; tunnel-on has a forward speed of 56 m/s, which is at the lower end of the OV-1B/JT15D operation range. Forward speed resulted in about a 10 dB reduction for the engine and wing-in configuration at the blade passage frequency. However, only part of this reduction was due to forward speed as seen by the engine only, 4-m/s spectra. Removal of the wing, by itself, amounted to a 5 dB reduction at the low forward speed. In contrast, at the high forward speed, removal of the wing did not significantly effect the BPF tone level.

*Blade-Mounted Transducer Spectra*

The effect of the wing on blade fluctuating pressure spectra is shown in Fig. 21. Note that the two BMT spectra at 56 m/s are similar as were the noise spectra of Fig. 20. These results indicate there are no apparent installation effects due to the OV-1 wing and turboprop at high forward speed. In contrast, the spectra at the tunnel minimum speed of 4 m/s show higher broadband levels and peaks for harmonic orders less than about 20. With the engine alone at low tunnel speed, unsteady disturbances due to tunnel turbulence are present. The addition of the wing results in additional unsteady disturbances being drawn into the inlet, probably not unlike that found to be present for static test stand support structures. Both of these unsteady disturbances on the fan blade may show up in the far field as an increase in noise level at the blade passage frequency.

## IV. Conclusions

Tests have been performed on a JT15D-1 turbofan engine both statically and at simulated forward speed in a wind tunnel. Based on an analysis of far-field acoustic data and fan blade-mounted transducer pressure data, the following conclusions have been reached.

1) Relative to results obtained from a static test stand, a sound power reduction on the order of 10 dB was achieved at

the blade passage frequency in the forward arc through simulated forward speed in the wind tunnel.

2) The sound power reduction resulted from a lessening of rotor-turbulence interaction and was primarily accomplished at a simulated speed of 10 m/s. Further increases in speed produced little additional sound power reduction.

3) The interaction of the rotor with a 6-per-revolution circumferential varying pressure field produced by downstream structural support struts internal to the engine is believed to be the dominant blade passage frequency source mechanism at simulated forward speed for high subsonic fan speeds.

4) Varying inlet angle of attack had little effect on the fan blade spectra and far-field acoustic directivity.

5) There was no apparent installation effect at forward speed in the forward quadrant due to the addition of a wing/engine assembly (OV-1) representative of an ongoing flight effects program.

## References

[1] McArdle, J.G., Jones, W.L., Heidelberg, L.J., and Homyak, L., "Comparison of Several Inflow Control Devices for Flight Simulation of Fan Tone Noise Using a JT15D-1 Engine," AIAA Paper 80-1025, June 1980.

[2] Hodder, B.K., "Further Studies of Static-to-Flight Effects on Fan Noise Using Inlet Distortion Control for Source Identification," NASA TM X-73183, Dec. 1976.

[3] Falarski, M.D. and Moore, M.T., "Acoustic Characteristics of Two Hybrid Inlets at Forward Speed," *Journal of Aircraft*, Vol. 17, Feb. 1980, pp. 106-111.

[4] Ahtye, W.F., "A Measurement of Forward-Flight Effects on the Noise from a JT15D-1 Turbofan Engine in the NASA Ames 40×80 foot Wind Tunnel," AIAA Paper 80-1026, June 1980.

[5] Hanson, D.B., "Study of Noise Sources in a Subsonic Fan Using Measured Blade Pressures and Acoustic Theory," NASA CR-2574, 1975.

[6] Gliebe, P.R. and Kerschen, E.J., "Analytical Study of the Effects of Wind Tunnel Turbulence and Fan Noise," NASA CR-152359, 1979.

[7] Schoenster, J.A., "Fluctuating Pressures on Fan Blades of a Turbofan Engine—Static and Wind Tunnel Investigations," NASA TP-1976, 1982.

[8] Englund, D.R., Grant, H.P., and Lanati, G.A., "Measuring Unsteady Pressure on Rotating Compressor Blades," NASA TM-79159, 1979.

[9] Mueller, A.W., "A Comparison of the Three Methods Used to Obtain Acoustic Measurements for the NASA Flight Effects Program," NASA TM-81906, Oct. 1980.

[10] Tyler, J.J. and Sofrin, T.G., "Axial Flow Compressor Noise Studies," *SAE Transactions*, Vol. 70, 1962, pp. 309-332.

[11] Rice, E.J., Heidmann, M.F., and Sofrin, T.G., "Model Propagation Angles in a Cylindrical Duct with Flow and Their Relation to Sound Radiation," NASA TM-79030, 1979.

[12] Heidmann, M.F., Saule, A.V., and McArdle, J.G., "Analysis of Radiation Patterns of Interaction Tones Generated by Inlet Rods in the JT15D Engine," AIAA Paper 79-0581, March 1979.